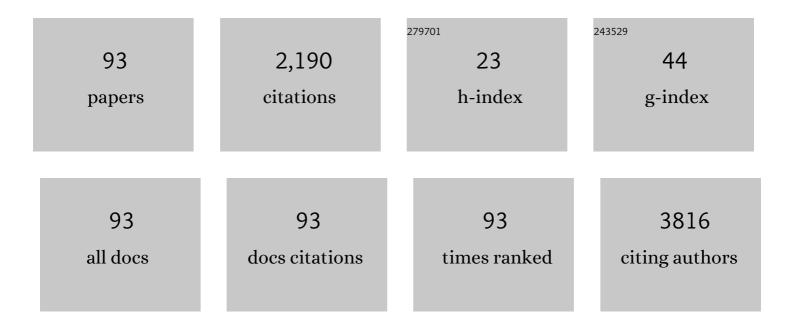
## List of Publications by Year in descending order

Source: https://exaly.com/author-pdf/5345964/publications.pdf Version: 2024-02-01



#	Article	IF	CITATIONS
1	Monolayer WS <sub>2</sub> Lateral Homosuperlattices with Two-dimensional Periodic Localized Photoluminescence. ACS Nano, 2022, 16, 597-603.	7.3	7
2	Temperature induced electrical transport in n-Bi2Te3/p-InAs thermoelectric heterojunctions. Journal of Materials Science, 2022, 57, 8767-8778.	1.7	0
3	Long-wavelength infrared selective emitter for thermal infrared camouflage under a hot environment. Optics Express, 2022, 30, 24132.	1.7	10
4	Ferroelectric dielectric and optical properties of layered PbZr <i><sub>x</sub></i> Ti <i><sub>1-x</sub></i> O <sub>3</sub> films derived from precursor solutions containing polyvinylpyrrolidone polymer additive. Ferroelectrics, 2021, 571, 120-128.	0.3	0
5	Bio-Separated and Gate-Free 2D MoS2 Biosensor Array for Ultrasensitive Detection of BRCA1. Nanomaterials, 2021, 11, 545.	1.9	7
6	Nonlocal effective-medium theory for periodic multilayered metamaterials. Journal of Optics (United) Tj ETQq0 0	0 rgBT /O	verlock 10 Tf
7	Observation of gain operation mode in Ge:B BIB THz detector. AIP Advances, 2021, 11, 055015.	0.6	1

8	Dark-Current-Blocking Mechanism in BIB Far-Infrared Detectors by Interfacial Barriers. IEEE Transactions on Electron Devices, 2021, 68, 2804-2809.	1.6	5
9	Tunable spatial-frequency-shift 3D nanoscopy with chip compatibility overcomes the diffraction limit of the linear optical imaging system. Science China: Physics, Mechanics and Astronomy, 2021, 64, 1.	2.0	0
10	Highâ€Performance Roomâ€Temperature Extendedâ€Wavelength InAsâ€Based Middleâ€Wavelength Infrared Photodetector. Physica Status Solidi (A) Applications and Materials Science, 2021, 218, 2100281.	0.8	5
11	Low Deposition Temperature Amorphous ALD-Ga <sub>2</sub> O <sub>3</sub> Thin Films and Decoration with MoS <sub>2</sub> Multilayers toward Flexible Solar-Blind Photodetectors. ACS Applied Materials & amp; Interfaces, 2021, 13, 41802-41809.	4.0	23
12	Dynamically reconfigurable subwavelength optical device for hydrogen sulfide gas sensing. Photonics Research, 2021, 9, 2060.	3.4	4
13	Remarkable photoluminescence enhancement of CsPbBr <sub>3</sub> perovskite quantum dots assisted by metallic thin films. Nanophotonics, 2021, 10, 2257-2264.	2.9	10
14	Evolution of Structural and Electronic Properties of TiSe <sub>2</sub> under High Pressure. Journal of Physical Chemistry Letters, 2021, 12, 9859-9867.	2.1	21
15	Discovery of Superconductivity in Mercury Cadmium Telluride. Journal of Physical Chemistry C, 2021, 125, 24746-24754.	1.5	Ο
16	Enhancement of Low-Temperature Gas-Sensing Performance Using Substoichiometric WO <sub>3–<i>x</i></sub> Modified with CuO. ACS Applied Materials & Interfaces, 2020, 12, 41230-41238.	4.0	19
17	Flexible Transparent Heat Mirror for Thermal Applications. Nanomaterials, 2020, 10, 2479.	1.9	4
18	Strained VO 2 Nanostructure Thin Films with an Unaffected Insulator–Metal Transition. Physica Status Solidi (B): Basic Research, 2020, 257, 1900785.	0.7	1

#	Article	IF	CITATIONS
19	Gas Sensing Performance and Mechanism of CuO(p)-WO3(n) Composites to H2S Gas. Nanomaterials, 2020, 10, 1162.	1.9	13
20	High-efficiency, low-cost distributed Bragg reflector based on Al2O3/PbZr0.4Ti0.6O3 multilayer. AlP Advances, 2020, 10, .	0.6	4
21	Ultrasensitive ppb-level H2S gas sensor at room temperature based on WO3/rGO hybrids. Journal of Materials Science: Materials in Electronics, 2020, 31, 5008-5016.	1.1	18
22	Impact of the Structural Parameters on the Photoresponse of Terahertz Blocked-Impurity-Band Detectors With Planar Structure. IEEE Transactions on Terahertz Science and Technology, 2020, 10, 358-362.	2.0	7
23	Magenta-Emitting Cesium Lead Halide Nanocrystals Encapsulated in Dimethicone for White Light-Emitting Diodes. ACS Applied Nano Materials, 2020, 3, 4886-4892.	2.4	10
24	Studies on Sensing Properties and Mechanism of CuO Nanoparticles to H2S Gas. Nanomaterials, 2020, 10, 774.	1.9	39
25	Wide gamut, angle-insensitive structural colors based on deep-subwavelength bilayer media. Nanophotonics, 2020, 9, 3385-3392.	2.9	16
26	<i>In situ</i> growth of ultrasmall cesium lead bromine quantum dots in a mesoporous silica matrix and their application in flexible light-emitting diodes. Nanoscale, 2019, 11, 16499-16507.	2.8	47
27	Largeâ€Area, Broadband, Wideâ€Angle Plasmonic Metasurface Absorber for Midwavelength Infrared Atmospheric Transparency Window. Advanced Optical Materials, 2019, 7, 1900841.	3.6	44
28	Layered Nonstoichiometric V <sub>7</sub> O <sub>16</sub> Thin Films with Controlled Oxygen-Deficient Multivalent States and Crystalline Phases. ACS Applied Electronic Materials, 2019, 1, 2308-2313.	2.0	1
29	Modulated Metal–Insulator Transition Behaviors in Vanadium Dioxide Nanowires with an Artificial Oxidized Domain. Physica Status Solidi - Rapid Research Letters, 2019, 13, 1900383.	1.2	8
30	Alâ€Đopingâ€Induced VO <sub>2</sub> (B) Phase in VO <sub>2</sub> (M) Toward Smart Optical Thin Films with Modulated Δ <i>T</i> <sub>vis</sub> and Δ <i>T</i> <sub>c</sub> . Advanced Engineering Materials, 2019, 21, 1900947.	1.6	19
31	Suppression of Photoinduced Surface Oxidation of Vanadium Dioxide Nanostructures by Blocking Oxygen Adsorption. ACS Omega, 2019, 4, 17735-17740.	1.6	6
32	Phonon Anharmonicity of Tungsten Disulfide. Journal of Physical Chemistry C, 2019, 123, 25509-25514.	1.5	12
33	Controllable Polarization Rotator with Broadband High Transmission Using Allâ€Dielectric Metasurfaces. Advanced Theory and Simulations, 2019, 2, 1900086.	1.3	24
34	Structural, vibrational, electrical, and magnetic properties of mixed spinel ferrites Mg1-xZnxFe2O4 nanoparticles prepared by co-precipitation. AIP Advances, 2019, 9, .	0.6	22
35	Nonstoichiometric Oxygenâ€Đependent Microstructures and Phase Transitions in Postâ€Annealed Vanadium Dioxides. Advanced Engineering Materials, 2019, 21, 1801374.	1.6	9
36	Giant conductivity enhancement: Pressure-induced semiconductor-metal phase transition in Cd0.90Zn0.1Te. Physical Review B, 2019, 99, .	1.1	6

#	Article	IF	CITATIONS
37	Improving gas sensing performance by oxygen vacancies in sub-stoichiometric WO <sub>3â^'x</sub> . RSC Advances, 2019, 9, 7723-7728.	1.7	52
38	Strained 2D Layered Materials and Heterojunctions. Annalen Der Physik, 2019, 531, 1800465.	0.9	20
39	Large-area, lithography-free, narrow-band and highly directional thermal emitter. Nanoscale, 2019, 11, 19742-19750.	2.8	39
40	Excitonic Luminescence Engineering in Tervalent-Europium-Doped Cesium Lead Halide Perovskite Nanocrystals and Their Temperature-Dependent Energy Transfer Emission Properties. Journal of Physical Chemistry C, 2018, 122, 29044-29050.	1.5	33
41	Phonon replicas of type-II GaSb/GaAs quantum dot structure grown by liquid phase epitaxy. Applied Physics A: Materials Science and Processing, 2018, 124, 1.	1.1	Ο
42	Selectedâ€Area Chemical Nanoengineering of Vanadium Dioxide Nanostructures Through Nonlithographic Direct Writing. Advanced Materials Interfaces, 2018, 5, 1800974.	1.9	11
43	Spatial and Frequency Selective Plasmonic Metasurface for Long Wavelength Infrared Spectral Region. Advanced Optical Materials, 2018, 6, 1800337.	3.6	23
44	Optical Properties of Al-Doped ZnO Films in the Infrared Region and Their Absorption Applications. Nanoscale Research Letters, 2018, 13, 149.	3.1	26
45	Temperature-dependent Photoluminescence of Silicon Nanocrystals Embedded in SiO2 Matrix. Chemical Research in Chinese Universities, 2018, 34, 513-516.	1.3	Ο
46	PbZr <sub>0.4</sub> Ti <sub>0.6</sub> O <sub>3</sub> dielectric reflectors with large photonic band gap and high average optical reflectivity. Journal of the American Ceramic Society, 2017, 100, 1275-1279.	1.9	1
47	Optical Constants and Band Gap Evolution with Phase Transition in Sub-20-nm-Thick TiO2 Films Prepared by ALD. Nanoscale Research Letters, 2017, 12, 243.	3.1	30
48	The effect of infrared plasmon on the performance of Si-based THz detectors. Journal of Materials Science: Materials in Electronics, 2017, 28, 839-844.	1.1	13
49	Photoelectrochemical Complexes of Fucoxanthinâ€Chlorophyll Protein for Bioâ€Photovoltaic Conversion with a High Openâ€Circuit Photovoltage. Chemistry - an Asian Journal, 2017, 12, 2996-2999.	1.7	7
50	A Universal Route to Realize Radiative Cooling and Light Management in Photovoltaic Modules. Solar Rrl, 2017, 1, 1700084.	3.1	78
51	Electrical and optical properties of a kind of ferroelectric oxide films comprising of PbZr0.4Ti0.6O3 stacks. Journal of Applied Physics, 2017, 122, 024102.	1.1	1
52	Surface plasmon enhanced Si-based BIB terahertz detectors. Applied Physics Letters, 2017, 111, .	1.5	13
53	Tailor the functionalities of metasurfaces based on a complete phase diagram. , 2016, , .		2
54	Bulk photovoltaic effect at infrared wavelength in strained Bi2Te3 films. APL Materials, 2016, 4, .	2.2	9

#	Article	IF	CITATIONS
55	CuO/WO <sub>3</sub> Hybrid Nanocubes for Highâ€Responsivity and Fastâ€Recovery H <sub>2</sub> S Sensors Operated at Low Temperature. Particle and Particle Systems Characterization, 2016, 33, 15-20.	1.2	23
56	Thickness-Dependent Optical Constants and Annealed Phase Transitions of Ultrathin ZnO Films. Journal of Physical Chemistry C, 2016, 120, 22532-22538.	1.5	14
57	Shaping the flow of light based on abrupt phase discontinuities operation in high order modes. , 2016, , .		0
58	Anomalous thermoelectricity in strained Bi2Te3 films. Scientific Reports, 2016, 6, 32661.	1.6	11
59	Effects of Al Doping on the Properties of ZnO Thin Films Deposited by Atomic Layer Deposition. Nanoscale Research Letters, 2016, 11, 407.	3.1	95
60	Interlayer Transition and Infrared Photodetection in Atomically Thin Type-II MoTe <sub>2</sub> /MoS <sub>2</sub> van der Waals Heterostructures. ACS Nano, 2016, 10, 3852-3858.	7.3	453
61	Tailor the Functionalities of Metasurfaces Based on a Complete Phase Diagram. Physical Review Letters, 2015, 115, 235503.	2.9	230
62	Plasmonic metasurfaces: From perfect absorption to phase modulation. , 2015, , .		0
63	Zn-aided defect control for ultrathin GZO films with high carrier concentration aiming at alternative plasmonic metamaterials. Physica Status Solidi (A) Applications and Materials Science, 2015, 212, 1713-1718.	0.8	18
64	Self-Induced Uniaxial Strain in MoS <sub>2</sub> Monolayers with Local van der Waals-Stacked Interlayer Interactions. ACS Nano, 2015, 9, 2704-2710.	7.3	47
65	Surface properties of AlN and Al x Ga1â^'x N epitaxial layers characterized by angle resolved X-ray photoelectron spectroscopy. Journal of Materials Science: Materials in Electronics, 2015, 26, 950-954.	1.1	6
66	An effective way to simultaneous realization of excellent optical and electrical performance in largeâ€scale Si nano/microstructures. Progress in Photovoltaics: Research and Applications, 2015, 23, 964-972.	4.4	29
67	Vertically coupled ZnO nanorods on MoS2 monolayers with enhanced Raman and photoluminescence emission. Nano Research, 2015, 8, 743-750.	5.8	52
68	Flexible transparent conductive films on PET substrates with an AZO/AgNW/AZO sandwich structure. Journal of Materials Chemistry C, 2014, 2, 3750-3755.	2.7	50
69	GROWTH AND MICROSTRUCTURES OF ULTRATHIN <font>Bi</font> <sub>2</sub> <font>Te</font> <sub>3</sub> NANOPLATES BY MODIFIED HOT WALL EPITAXY. Nano, 2014, 09, 1450056.	0.5	4
70	Raman mapping of laser-induced changes and ablation of InAs nanowires. Applied Physics A: Materials Science and Processing, 2014, 115, 885-893.	1.1	4
71	Sol–gel derived near-UV and visible antireflection coatings from hybridized hollow silica nanospheres. Journal of Sol-Gel Science and Technology, 2014, 71, 267-275.	1.1	47
72	Light-harvesting complex II sensitized oxide photoanodes with organic acceptor molecule as electron transfer mediator. Chemical Research in Chinese Universities, 2014, 30, 181-184.	1.3	2

#	Article	IF	CITATIONS
73	Vapor-deposited amorphous metamaterials as visible near-perfect absorbers with random non-prefabricated metal nanoparticles. Scientific Reports, 2014, 4, 4850.	1.6	40
74	Application of three-dimensionally area-selective atomic layer deposition for selectively coating the vertical surfaces of standing nanopillars. Scientific Reports, 2014, 4, 4458.	1.6	28
75	Radial sandwich hybrid nanorods by analogously inserting Au nanoparticles in ZnO nanorods. RSC Advances, 2013, 3, 21256.	1.7	0
76	Controllable synthesis of WO3•nH2O microcrystals with various morphologies by a facile inorganic route and their photocatalytic activities. New Journal of Chemistry, 2013, 37, 1538.	1.4	61
77	Controllable Synthesis of Cu <sub>2</sub> In <sub>2</sub> ZnS <sub>5</sub> Nano/Microcrystals and Hierarchical Films and Applications in Dye-Sensitized Solar Cells. Journal of Physical Chemistry C, 2013, 117, 10296-10301.	1.5	30
78	Nanosphere@nanorod hybrid arrays generated on substrates by a one-pot process as low-reflecting surfaces. RSC Advances, 2013, 3, 21039.	1.7	2
79	Multilayer Hybrid Structure of ZnO Nanorod Arrays Imbedded in TiO2 Network as Photoanode. Materials Research Society Symposia Proceedings, 2013, 1493, 111-116.	0.1	0
80	Nondestructively decorating surface textured silicon with nanorod arrays for enhancing light harvesting (Phys. Status Solidi A 12â^•2013). Physica Status Solidi (A) Applications and Materials Science, 2013, 210, .	0.8	0
81	Nondestructively decorating surface textured silicon with nanorod arrays for enhancing light harvesting. Physica Status Solidi (A) Applications and Materials Science, 2013, 210, 2542-2549.	0.8	6
82	A solution synthetic route toward Bi <sub>2</sub> Se <sub>3</sub> layered nanostructures with tunable thickness via weakening precursor reactivity. Physica Status Solidi (A) Applications and Materials Science, 2013, 210, 1909-1913.	0.8	5
83	Logic Circuit Function Realization by One Transistor. Nano Letters, 2012, 12, 5954-5956.	4.5	15
84	Terahertz coherent control of surface plasmon polariton propagation in subwavelength metallic hole arrays. Applied Physics Letters, 2012, 100, .	1.5	8
85	The Extraordinary Transmission Spectrum in Terahertz Regime: Combination of Shape Resonances and Rayleigh anomalies. Journal of Infrared, Millimeter, and Terahertz Waves, 2012, 33, 212-217.	1.2	3
86	Surface plasma resonance spectra of Au nanoparticles formed from dewetted thin films. Journal of Materials Science, 2012, 47, 668-676.	1.7	12
87	A Special Configuration of Lead Zirconate Titanate Multilayer Stack with Superior Electrical and Optical Properties. Journal of the American Ceramic Society, 2011, 94, 2761-2763.	1.9	3
88	Colloidal Cu <sub>2</sub> ZnSnS <sub>4</sub> nanocrystals generated by a facile route using ethylxanthate molecular precursors. Physica Status Solidi - Rapid Research Letters, 2011, 5, 113-115.	1.2	35
89	Weak antilocalization effect in high-mobility two-dimensional electron gas in an inversion layer on p-type HgCdTe. Applied Physics Letters, 2011, 99, .	1.5	9
90	Effect of Polyethylene Glycol Content on the Optical Properties of Ba <sub>0.9</sub> Sr <sub>0.1</sub> TiO <sub>3</sub> Multilayers. Journal of the American Ceramic Society, 2009, 92, 539-541.	1.9	3

#	Article	IF	CITATIONS
91	Construction of PbZr <sub>0.4</sub> Ti <sub>0.6</sub> O <sub>3</sub> â€and Ba <sub>0.9</sub> Sr <sub>0.1</sub> TiO <sub>3</sub> â€Based Optical Microcavities by Chemical Solution Deposition. Journal of the American Ceramic Society, 2009, 92, 2159-2161.	1.9	2
92	Influence of nonlinear effects in ZnTe on generation and detection of terahertz waves. Journal of Applied Physics, 2009, 105, .	1.1	13
93	Carrier concentration dependence of terahertz transmission on conducting ZnO films. Applied Physics Letters, 2008, 93, .	1.5	40